Review

Quantifying chaos of curvilinear beams via exponents

J. Awrejcewicz [b,c,*], V.A. Krysko [a], I.E. Kutepov [a], I.Yu. Vygodchikova [a], A.V. Krysko [d]

[a] Department of Mathematics and Modeling, Saratov State Technical University, Politehnicheskaya 77, 410054 Saratov, Russian Federation
[b] Department of Automation, Biomechanics and Mechatronics, Lodz University of Technology, 1/15 Stefanowski Str., 90-924 Lodz, Poland
[c] Institute of Vehicles, Warsaw University of Technology, 84 Narbutt Str., 02-524 Warsaw, Poland
[d] Department of Applied Mathematics and Systems Analysis, Saratov State Technical University, Politehnicheskaya 77, 410054 Saratov, Russian Federation

ARTICLE INFO

ABSTRACT

We propose a procedure for predicting the stability loss and transition into chaos of a network of oscillators lying on a curve, where each of the oscillators can move in two perpendicular directions. Dynamics of the coupled oscillators are governed by the sixth-order PDE, which is directly derived using the classical hypotheses of a curvilinear flexible beam movement theory. We apply FDM (Finite Difference Method) to reduce PDEs into ODEs, and the used number of spatial coordinate positions defines the number of involved oscillators approximating the dynamics of our continuous structural member (beam). Our procedure has a few advantages over the classical approaches, which has been illustrated and discussed. The proposed method has been validated for non-linear dynamical regimes by using the classical vibrational analysis (time histories, frequency power spectra and Poincaré maps).

© 2015 Elsevier B.V. All rights reserved.

Contents

* Corresponding author at: Department of Automation, Biomechanics and Mechatronics, Lodz University of Technology, 1/15 Stefanowski Str., 90-924 Lodz, Poland.
   E-mail addresses: awrejcew@p.lodz.pl (J. Awrejcewicz), tak@san.ru (V.A. Krysko), iekutepov@gmail.com (I.E. Kutepov), VigodchikovaIY@info.sgu.ru (I.Yu. Vygodchikova), anton.krysko@gmail.com (A.V. Krysko).

1. Introduction

We are motivated here by the recent trends of research in social sciences, where human events/dynamics exhibit high complexity in comparison to physical sciences. A key role in social sciences play measures and indicators used to control and possibly to predict the social complex reality including events beyond time and space (social, cultural and psychological factors certainly influence the obtained results [1]).

There is a wide range of individual indicators which are associated with various complex structural changes of social development including public health, sustainable production and consumption, transport, climate change, etc. There is no hope to take into account all of these events, so only a few most adaptable and reliable indicators are usually applied. For example, in the case of economic activity the price or currency value can be used only. The reduction of complex social problems to a few successful indicators may yield an effective composite measure which is simultaneously simple and universal. Then, this appropriately chosen quantification indicator can also be used in other fields of human activity like housing, transactions or communication.

On the other hand, a lot of ideas to identify and quantify fundamental features of the time-evolution of self-organizing complex dynamical systems like financial market came from theoretical physics. For instance, the random matrix theory can be successfully applied to analyze the stock market correlation matrix [2]. Recurrence plots and recurrence quantification analysis are applied to monitor the dynamics of stock prices in emerging markets [3].

It should be mentioned that the applied indices (for instance the Dow Jones index) in social sciences as well as weather and climate predictions may exhibit *fractal* fluctuations on different time scales. The well-known characteristics borrowed from the theory of non-linear dynamical systems like *power spectra* or *fractal fluctuations*, *golden mean motion* as well as primary *perturbation time periods* measured by days, months and years are applied to quantify the total *space-temporal* social event patterns.

There is a strong interrelation between non-linear physical dynamical phenomena and data sets of complex social processes (structural changes, wars, shocks, political crises, etc.). Before 1980s only the theoretical background of regular dynamics was applied directly to predict deviations from the trends of growth generated by endogenous shocks arising from imperfections of the market [4]. However, it was discovered that the real economic time-series representing time histories of the used indicators had not only broad band frequency spectra, but also different amplitudes, and revealed other non-linear phenomena including *jumps*, time *irreversibility, non-regular waves, asymmetries* and so on, typical of non-linear behavior observed in mechanical structural members like beams and plates/shells [5,6].

In reference [7] it is indicated that rich dynamical behavior of economics data sets being outcomes of the above listed structural processes shows structural instability effects and complex non-linear dynamical behavior, including periodicity, quasi-periodicity and chaos (see also [8]).

The method of research presented in this paper as well as results obtained are based on an interaction between the ideas regarding dynamical processes taking place in the applied Physics/Mechanics and Economics. However, contrary to the classical (still existing) trends observed in economy relying on applications of the theoretical background developed in applied mathematics, physics and mechanics, we use rather an inverse way of research, since the ideas originated from a study of time series governing non-linear dynamical phenomena of various economic events. The presented approach is motivated by recent trends in studies on behavior and analysis of complex systems dynamics. Namely, in order to achieve a quantitative description of dynamical properties, only a limited number of system parameters is used. In general, the description and quantification of random functions require analysis of data of millions of points of the dynamical systems coming from various branches of pure and applied sciences. Since the results are influenced by various errors associated with the use of numerical approaches applied, other qualitatively different approaches are highly required.

Recently, the concept of an *intermediate* model [9], when the "best fit" model is unavailable, has been proposed using two general principles. One of them is based on self-similar properties of the studied long-time series [9], while another one aims at detection of quasi-periodic processes [10] via the so called Prony decomposition approach. Note that the latter one applies the conventional Fourier transformation as a *partial* case. The Prony decomposition and the Prony spectrum are used to describe quantitatively a wide class of random functions. In paper [11] a chaotic system exhibited by a triple physical pendulum with one, two and three positive Lyapunov's exponents was studied. Chaotic dynamics of the mentioned lumped mechanical systems was illustrated via amplitude–frequency response being extracted from the corresponding generalized Prony spectrum, and was used as a specific "fingerprint" characterizing the random behavior of the triple-pendulum system. It has been shown that the latter quantitative presentation of random date yields additional possibilities in classifying chaotic and random behaviors of complex systems.

Motivated by the so far described approach, we present a method for fast and reliable prediction of stability loss in a thin curvilinear beam. The study of the beam, which usually is a member of thin-walled structures, plays a key role in solving various problems related to non-linear phenomena and stability (see the state-of-art of the stability problems regarding strongly non-linear systems in monograph [12]).

In this paper our aim is not to give theorems and their proofs regarding the fundamental question how one can find completely rigorous results claiming chaos in a nonlinear system. However, we have solved the problem how well one can find rigorous results regarding numerical quantifications of the system of ODEs governing dynamics of curvilinear beams. Using the classical numerical analysis, we have shown examples of chaotic attractors which have been validated numerically.

Here, flexibility index E_T and deflection indicator I are applied to estimate the most suitable parameters characterizing a transition of the flexible curvilinear beams from regular to chaotic dynamics. Next, we illustrate the mentioned novel approach versus classical methods in order to predict the transition into chaotic dynamics via rather simple approach, and we study the principal peculiarities and advantages of each of the mentioned methods.

Traditionally, the elasticity/flexibility indicators are applied in micro-economics to analyze problems on financial and commodity markets [13,14]. Knowledge of the theory of the mentioned indexes is required for marketing services. It gives a possibility to construct a proper price strategy, as well as to predict the decrease or increase of prices in order to achieve the required targets. The second application of the used theory is associated with a governing politics of taxes. Since the estimation of indicators requires a rigorous mathematical treatment [15], it is rational to extend the space of application of these useful indicators to dynamics of engineering objects.

The paper structure is organized in the following way. After *Introduction*, in Section 2 the classical approaches aimed on the analysis of chaotic time series are illustrated and discussed including the beam mathematical model, analysis via time series, Lyapunov exponents and Poincaré maps. Then, in Section 3, the method of indexing is introduced followed by a computational experiment. Concluding remarks (Section 4) finish the paper.

2. Classical approaches

2.1. Mathematical model of the beam

We consider a flexible one-layer thin curvilinear beam of length a, height h and curvature k_x of its middle plane. The beam is loaded by continuous load $q(x,t) = q_0 \sin(\omega_p t)$, where x stands for a horizontal axis and coordinate z goes down in the direction normal to the beam (see Fig. 2.1). Here q_0 is the amplitude of excitation, and ω_p is the excitation frequency.

The mathematical model of the beam is governed by a system of non-linear non-dimensional PDEs, and is derived using the following hypotheses:

(i) an arbitrary transversal cross section normal to the middle beam surface remains straight and normal to this surface after deformation, and the beam cross section remains unaffected;
(ii) we apply here the Euler–Bernoulli beam model and Kármán non-linearity; the beam material is elastic;
(iii) inertial effects of rotation of the beam elements are not taken into account, but the inertial forces responsible for displacement along the beam normal direction are taken into consideration;
(iv) external forces change their directions during the beam deformation.

The governing equations are as follows

$$\frac{1}{\lambda^2}\left\{-\frac{1}{12}\frac{\partial^4 w}{\partial x^4} + k_x\left[\frac{\partial u}{\partial x} - k_x w - \frac{1}{2}\left(\frac{\partial w}{\partial x}\right)^2 - w\frac{\partial^2 w}{\partial x^2}\right] + +L_1(u,w) + L_2(w,w)\right\} + q - \frac{\partial^2 w}{\partial t^2} - \varepsilon\frac{\partial w}{\partial t} = 0,$$

$$\frac{\partial^2 u}{\partial x^2} - k_x\frac{\partial w}{\partial x} + L_3(w,w) - \frac{\partial^2 u}{\partial t^2} = 0,$$

(2.1)

where: $L_1(u,w) = \frac{\partial^2 u}{\partial x^2}\frac{\partial w}{\partial x} + \frac{\partial u}{\partial x}\frac{\partial^2 w}{\partial x^2}$; $L_2(w,w) = \frac{3}{2}\left(\frac{\partial w}{\partial x}\right)^2\frac{\partial^2 w}{\partial x^2}$; $L_3(w,w) = \frac{\partial w}{\partial x}\frac{\partial^2 w}{\partial x^2}$; $w(x,t)$ – beam normal deflection; $u(x,t)$ – beam longitudinal deflection; ε – damping coefficient; $\lambda = a/h$; $k_x = \frac{1}{R_x}$ – curvature; $L_1(u,w)$, $L_2(w,w)$ and $L_3(w,w)$ – non-linear operators.

The correspondence between dimensional and non-dimensional parameters is as follows (note that bars over non-dimensional quantities in (2.1) are already omitted)

$$\lambda = \frac{a}{h}, \quad \bar{w} = \frac{w}{h}, \quad \bar{u} = \frac{ua}{h^2}, \quad \bar{x} = \frac{x}{a}, \quad \bar{t} = \frac{t}{\tau}, \quad \tau = \frac{a}{c},$$

$$c = \sqrt{\frac{Eg}{\gamma}}, \quad \bar{\varepsilon} = \frac{a}{c}, \quad \bar{q} = \frac{qa^4}{h^4 E}, \quad \bar{k}_x = \frac{k_x a}{\lambda}.$$

(2.2)

Eq. (2.1) should be supplemented by boundary conditions. We take the following conditions corresponding to stiff clamping of one beam end and a simple support of its remaining end
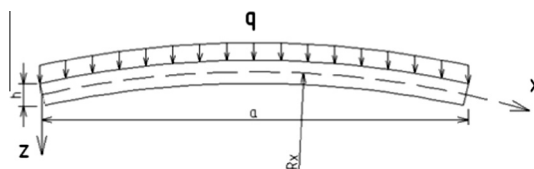

Fig. 2.1. Scheme of the curvilinear beam.

$$w(0,t) = w(a,t) = u(0,t) = u(a,t) = w'_x(0,t) = w''_x(a,t) = 0. \tag{2.3}$$

The following initial conditions are applied

$$w(x,0) = \dot{w}(x,0) = u(x,0) = \dot{u}(x,0) = 0. \tag{2.4}$$

In order to reduce PDEs (2.1) to ODEs we introduce the mesh

$$G_N = \{0 \le x_i \le 1, \ x_i = i/n, \ i = 0,\dots,n\},$$

and we apply the Taylor series in the neighborhood of x_i. We introduce the following difference operators with approximation $O(c^2)$, where c is the step of spatial coordinate:

$$\Lambda_x(\cdot_i) = \frac{(\cdot)_{i+1} - (\cdot)_{i-1}}{2c},$$

$$\Lambda_{x^2}(\cdot_i) = \frac{(\cdot)_{i+1} - 2(\cdot)_i + (\cdot)_{i-1}}{c^2},$$

$$\Lambda_{x^4}(\cdot_i) = \frac{(\cdot)_{i+2} - (\cdot)_{i+1} + 6(\cdot)_i - (\cdot)_{i-1} + (\cdot)_{i-2}}{c^4}.$$

Finally, we obtain the second-order ODEs with respect to time in the following form

$$\ddot{w}_t + \varepsilon \dot{w}_t = \lambda^2 \left\{ -\frac{1}{12}\Lambda_{x^4}(w_i) + k_x[\Lambda_x(u_i) - k_x w_i - w_i \Lambda_{x^2}(w_i)] + \Lambda_{x^2}(u_i)\Lambda_x(w_i) + \Lambda_{x^2}(w_i)\Lambda_x(u_i) + \frac{3}{2}(\Lambda_x(w_i))^2 \Lambda_{x^2}(w_i) + q \right\},$$

$$\ddot{u}_t = \Lambda_{x^2}(u_i) - k_x \Lambda_x(w_i) + \Lambda_x(w_i)\Lambda_{x^2}(w_i). \tag{2.5}$$

System of Eq. (2.5) is reduced to the first-order ODEs, and then it is solved via the fourth-order Runge–Kutta method. Boundary conditions require also difference approximation. The obtained mathematical model can be viewed as an approximation to problem (2.1). It is clear that its non-dimensional form allows us to go beyond the previously studied mechanical structural members and to fit remaining sciences, including economy. In addition, the truncated set of the second-order ODEs has also a general physical interpretation. Namely, the second-order ODEs define the dynamics of networks of homogenous oscillators placed on part of the curve which exhibits two perpendicular movements in u and w directions. The so far known topologies of the studied networks of oscillators include: (i) a ring or line of oscillators [16–18]; (ii) 2D array of oscillators [19]; (iii) all-to-all coupled network of oscillators [20]; (iv) all-to-all coupled oscillators of two subnetworks, where coupling takes place within a subnetwork and between two subnetworks [21].

Here, our aim is to investigate the novel network of coupled oscillators which generalizes the so far studied ring or line oscillators (observe that we may remove curvature of the network topology to get a line or to modify it to get a ring). Contrary to the all so far studied networks of oscillators, in our case the studied oscillator of the network may move in two directions, i.e. horizontal (u) and vertical (w). It means that each of the oscillators located on the curve part has two degrees of freedom. The introduced non-linearities are originated from the hypotheses and principles of Mechanics which are reliable and validated.

Our methodology and approach differ from the mentioned papers devoted to the study of networks of oscillators (their origin relies on artificial constructions of purely mathematical objects like maps or coupled ODEs, and then there is an attempt to validate their existence in biology, economy or a physical world). Since our model comes directly from physics/mechanics, also all introduced non-linearities and coupling which occur in the network of oscillators have their natural origin. The non-linear operators exhibit non-linear interactions either within one direction (L_2 and L_3) or between movements in two different directions (L_1). The curve part network of oscillators, contrary to the previously studied cases (i)–(iv), is subjected to the action of uniformly distributed harmonic excitation. The former can be interpreted as the action of periodic excitation at each of the non-linear oscillators which means that we study non-autonomous network.

This opens a door to extend the classical study of the networks of oscillators to real world behavior of social sciences, where the continuously acting external perturbation may come from rich human behavior out of the modeled networks. Furthermore, a number of the considered oscillators may change from 0 to n. It means that here we may study the dependence of mixed synchronous/incoherent systems configurations versus a number of interacting oscillators to get reliable and validated results. If we choose other n, then we may get (perhaps) interesting non-linear dynamical phenomena, but they will be beyond the dynamics governed by the studied PDEs. Furthermore, our goal is to predict spatio-temporal chaos in an efficient way. Note that difficulties in getting reliable results of the mechanical objects governed by PDEs, including computational time stability of the applied algorithm in time and spatial steps, etc. are widely described in references [22,23], and this discussion is omitted here.

The derived system of equations is extremely sensitive to the change of control parameters, i.e. even a negligible change of one of them may change qualitatively the system behavior. Therefore, by fixing control parameters $(q_0; \omega_p; \lambda; k_x)$ we may estimate reliability of the applied approaches based on getting the same numerical results. Since for our system we may get a few possible attractors, we may investigate convergence of each method at any possible attractor excluding transitional processes. Furthermore, validity of the results is estimated using qualitatively different methods to quantify the systems non-linear dynamics.

2.2. Time histories, Lyapunov spectra and Poincaré maps

In the case of periodic regime (Table 1) an increase in the number of oscillators n does not yield any quantitatively new results. The amplitude of response is changed only by 1–2%. Phase portraits exhibit an elliptical shape (not reported here), the Poincaré maps consist of one point, and the Fourier spectra contain sharp evidence of frequency $\omega_p = 5$.

Although for $q_0 = 60 \cdot 10^3$ (Table 2) the system is in a chaotic regime, which is indicated by time series, power spectra and Poincaré sections, one may observe convergence of the results up to $n = 90$. A further increase of the mesh nodes, i.e. the number of oscillators $[100, \ldots, 120]$ causes changes in the Poincaré section induced by errors introduced through numerical computations. The increase of partitions number produces new frequencies which were not observed earlier (this indicates the occurrence of unreliable results with respect to the modeled curvilinear flexible beam).

We have detected also a quasi-periodic regime (Table 3) for $\omega_p = 2.5$. For $q_0 = 60 \cdot 10^3$ the Fourier spectrum contains a series of linearly dependent frequencies which are irrational versus ω_p. For $n = 60$ there is a periodic attractor whose real existence has not been further validated. To sum up, the numerical simulations allow us to make a validated choice of the chains of oscillators composed of $n = 80$.

It should be emphasized, however, that in order to get validated results regarding a proper choice of the partitions number while applying FDM, we should first identify a vibrational regime. Namely, analysis of the Poincaré section shows that for different n we get different shapes of attractors which does not allow us to quantify the obtained results as reliable ones.

Next, we study the system transition into chaotic regime for $\omega_p = 5$. In the latter case we investigated time series, Fourier power spectra, phase portraits, deflection isoclines and the amplitude-time surface (not reported here, see for instance [22,23]). A comparison of the results was carried out for different values of control parameter q_0 with fixed frequency of $\omega_p = 5$ (the numerical results are reported in the tables).

Based on the computations presented in this paper and elsewhere, one may indicate the following drawbacks associated with the application of classical approaches to study non-linear dynamics of complex systems: (i) complexity in getting a

Table 1
Time histories, power spectra and Poincaré maps for $q_0 = 500$, $\omega_p = 5$, $\lambda = 50$, $k_x = 0$.
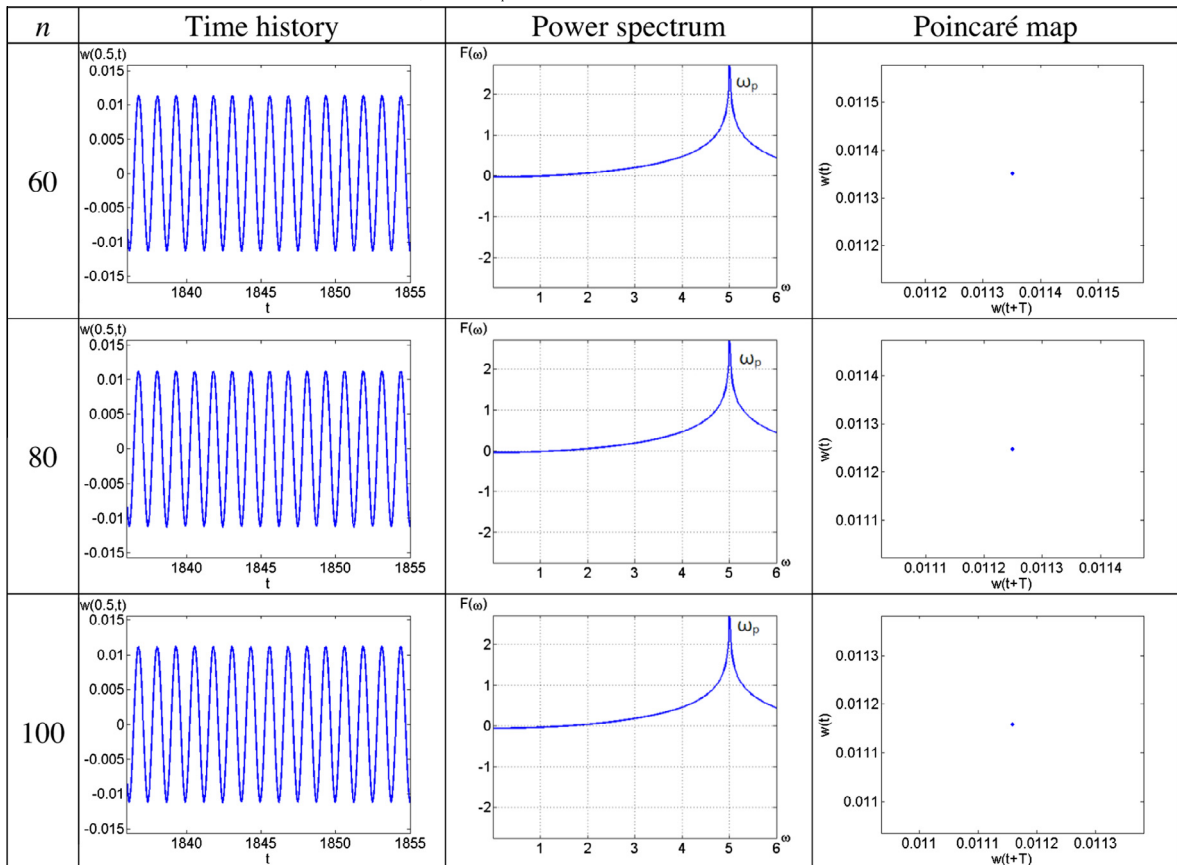
proper visualization of the attractor; (ii) essential dependence of the results on the involved number of oscillators n; (iii) the necessity of earlier estimation of the system vibration regime.

In order to avoid the above listed problems we propose to apply novel indicators which are particularly suitable for the validation of a chaotic regime.

Table 2
Time histories, power spectra and Poincaré maps ($q_0 = 60000$, $\omega_p = 5$, $\lambda = 50$, $k_x = 0$).
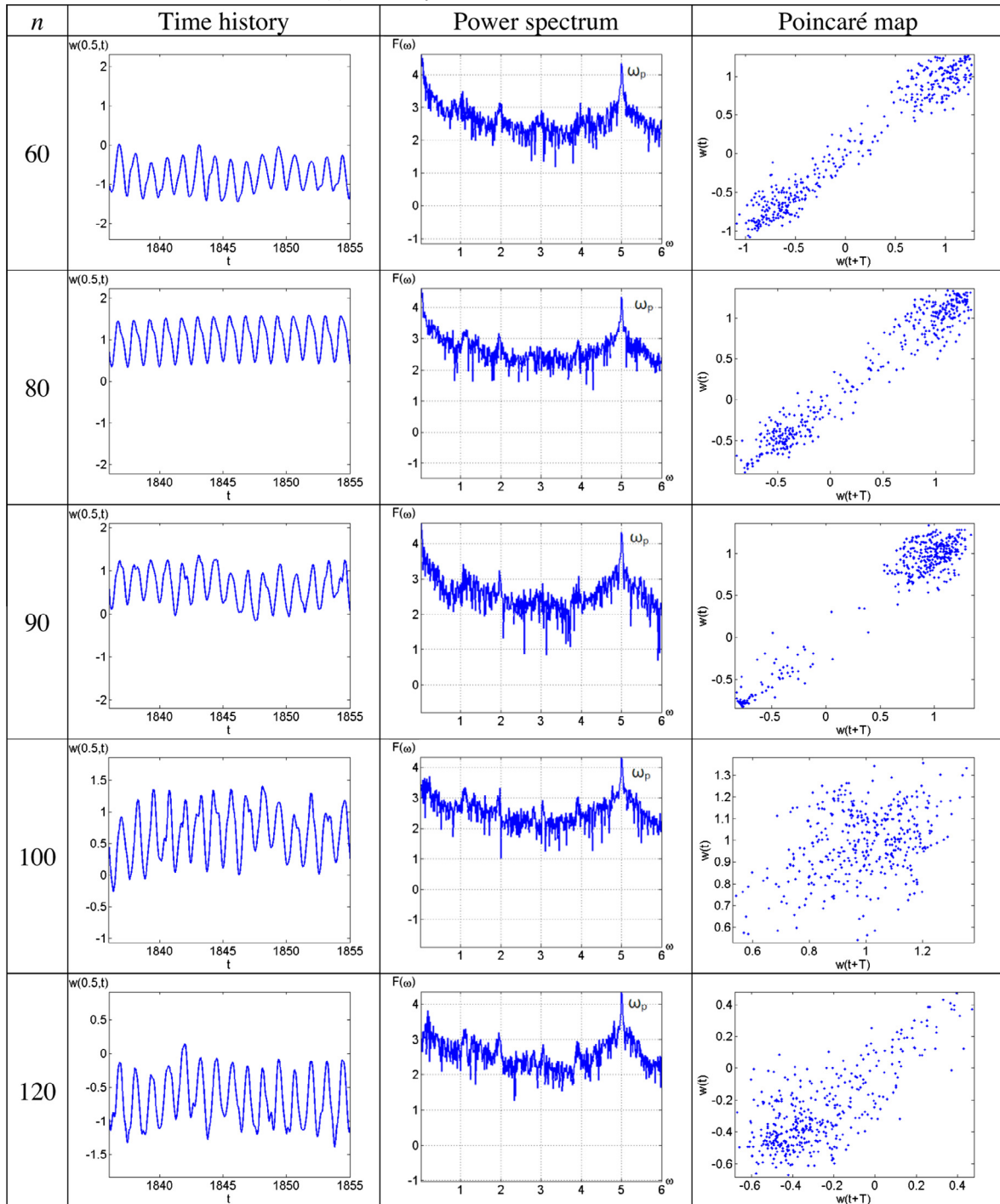
Table 3
Time histories, power spectra and Poincaré maps ($q_0 = 60000$, $\omega_p = 2.5$, $\lambda = 50$, $k_x = 0$).
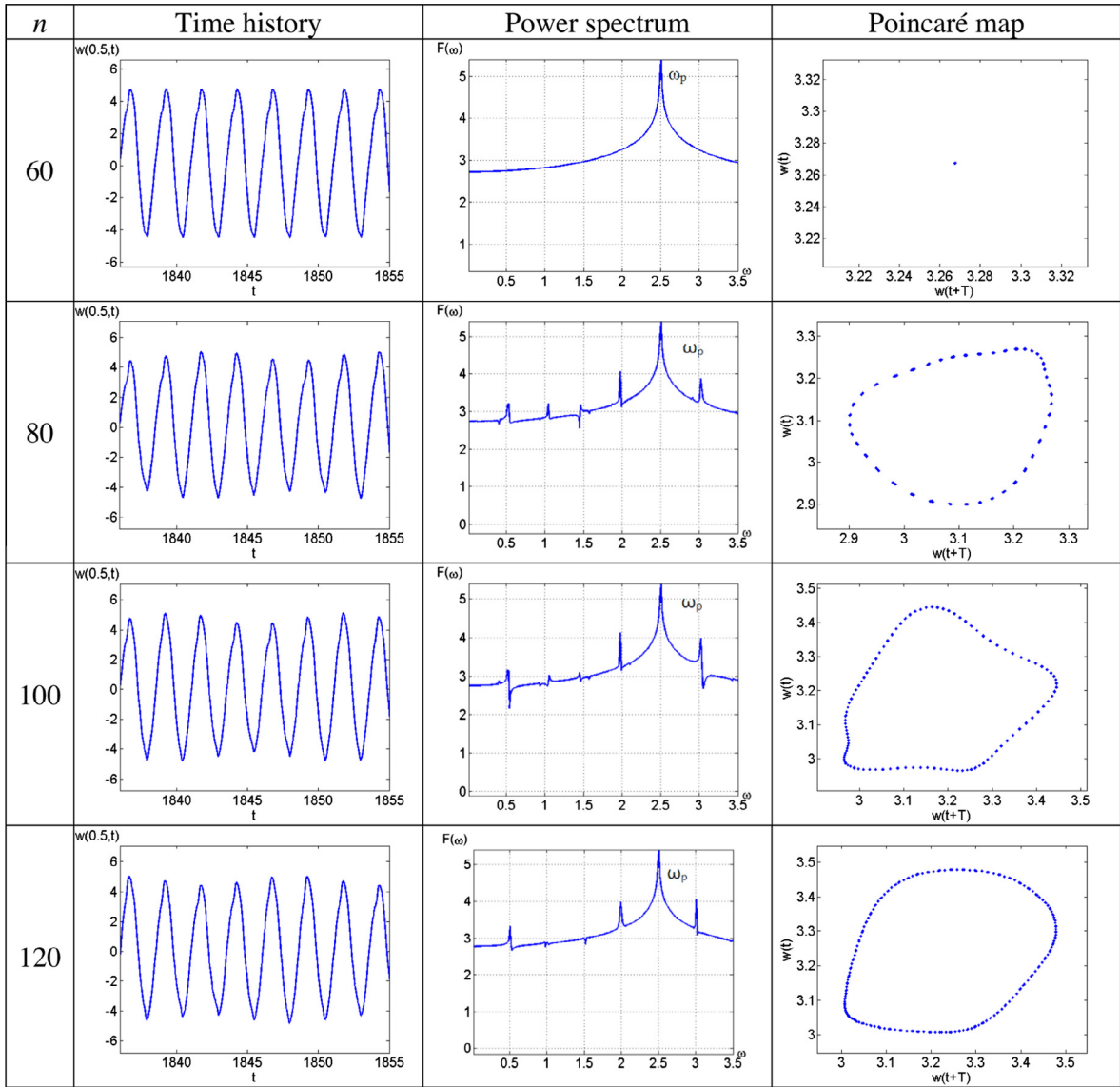
3. The method of elasticity

3.1. The proposed algorithm

Tables 4 and 5 give results of a computational experiment regarding the beam deflection amplitude versus the load $q = q_0 \sin \omega_p t$ ($\omega_p = 5$, $1836 < t < 2348$, $\Delta t = 1/256 = 0.00390625$) for the governing equations (2.1).

Then we use data from Tables 4 and 5 for modeling the estimated characteristics of process deflections using the new tools.

3.2. Application of the method

Consider discrete mesh $T = \{t_0 < t_1 < \cdots < t_N\}$, whose nodes n are associated with load functions $\{q(n, q_0, t_k)\}_{q_0 \in Q_0}^{n \in N_0}$ and deflection functions $\{w(n, q_0, t_k)\}_{q_0 \in Q_0}^{n \in N_0}$, $k = 0, \ldots, N$. In our experiment we took $N_0 = \{60, 80, 84, 88, 90, 94, 98\}$, $Q_0 = \{500, 60000\}$.

Table 4
Part of the initial data for $\omega_p = 5$, $n = 84$ (analogous data are obtained for $n = 60$, $n = 80$, $n = 88$, $n = 90$, $n = 94$, $n = 98$, $n = 100$, $n = 120$).

	n = 84					
	$q = q_0 \sin(\omega_p t)$	$q_0 = 500$		$q = q_0 \sin(\omega_p t)$	$q_0 = 60 \cdot 10^3$	
		t	w		t	w
1	135.30813	1836.00155	−0.00848	16236.97539	1836.00155	−0.63745
2	135.30813	1837.25819	−0.00848	16236.97540	1837.25819	−0.69475
3	135.30813	1838.51483	−0.00848	16236.97541	1838.51483	−0.43810
4	135.30813	1839.77146	−0.00848	16236.97542	1839.77146	−0.46614
5	135.30813	1841.02810	−0.00848	16236.97543	1841.02810	−0.52006
⋮	⋮	⋮	⋮	⋮	⋮	⋮
28	135.30813	1869.93075	−0.00848	16236.97567	1869.93075	−0.36081
29	135.30813	1871.18739	−0.00848	16236.97568	1871.18739	−0.35581
30	135.30813	1872.44403	−0.00848	16236.97569	1872.44403	−0.31018

Table 5
Part of the initial data for $\omega_p = 2.5$, $n = 84$ (analogous data are obtained for $n = 60$, $n = 80$, $n = 88$, $n = 90$, $n = 94$, $n = 98$, $n = 100$, $n = 120$).

	n = 84					
	$q = q_0 \sin(\omega_p t)$	$q_0 = 500$		$q = q_0 \sin(\omega_p t)$	$q_0 = 60 \cdot 10^3$	
		t	w		t	w
1	−70.607831	1836.00342	0.01342	16776.06236	1836.00342	−0.22165
2	−70.60783106	1838.51670	0.01342	16776.06237	1838.51670	−0.05671
3	−70.60783112	1841.02997	0.01342	16776.06238	1841.02997	0.27239
4	−70.60783118	1843.54324	0.01342	16776.06240	1843.54324	0.22862
5	−70.60783124	1846.05652	0.01342	16776.06241	1846.05652	−0.21029
⋮	⋮	⋮	⋮	⋮	⋮	⋮
25	−70.60783241	1896.32200	0.01342	16776.06268	1896.32200	−0.19435
26	−70.60783246	1898.83528	0.01342	16776.06269	1898.83528	0.00049
27	−70.60783252	1901.34855	0.01342	16776.06271	1901.34855	0.31709
28	−70.60783258	1903.86182	0.01342	16776.06272	1903.86182	0.15144
29	−70.60783264	1906.37510	0.01342	16776.06274	1906.37510	−0.25113
30	−70.60783270	1908.88837	0.01342	16776.06275	1908.88837	−0.15409

We introduce the normalized indexing load and deflection for $k = 0, \ldots, N$, where initial values of the functions taken in point t_0 for initial load q_0 serve as a basis

$$I_w(q_0, t_k) = w(n, q_0, t_k)/w(n, q_0, t_0), \tag{3.1}$$
$$I_q(q_0, t_k) = abs(q(n, q_0, t_k)/q(n, q_0, t_0)). \tag{3.2}$$

We apply formulas (3.1) and (3.2) for the given values of initial load $q_0 \in Q_0$:

$$I_w(500, t_k) = w(n, 500, t_k)/w(n, 500, t_0), \tag{3.3}$$
$$I_q(500, t_k) = abs(q(n, 500, t_k)/q(n, 500, t_0)), \tag{3.4}$$
$$I_w(60000, t_k) = w(n, 60000, t_k)/w(n, 60000, t_0), \tag{3.5}$$
$$I_q(60000, t_k) = abs(q(n, 60000, t_k)/q(n, 60000, t_0)). \tag{3.6}$$

The elasticity [13] shows approximately how the function value is changed (in percents) while changing the argument by 1%. The elasticity of deflection for each $k = 0, \ldots, N$ via the following formula

$$E(n, q_0, t_k) = \frac{I_w(q_0, t_k) - 1}{I_q(q_0, t_k) - 1} = \frac{\Delta w/w}{\Delta q/q}. \tag{3.7}$$

We apply formula (3.7) for the given values of initial load $q_0 \in Q_0$, and we get

$$E(n, 500, t_k) = \frac{w(n, 500, t_k)/w(n, 500, t_0) - 1}{q(n, 500, t_k)/q(n, 500, t_0) - 1},$$

$$E(n, 60000, t_k) = \frac{w(n, 60000, t_k)/w(n, 60000, t_0) - 1}{q(n, 60000, t_k)/q(n, 60000, t_0) - 1}.$$

Maximum estimation of the elasticity is

$$E_T(n, q_0) = \max_{k=0,\ldots,N} E(n, q_0, t_k). \tag{3.8}$$

We apply (3.8) for the given data of initial load $q_0^1 \in Q_0$, $q_0^2 \in Q_0$:

$$E_T(n, 500) = \max_{k=0,\dots,N} E(n, 500, t_k),$$
(3.9)

$$E_T(n, 60000) = \max_{k=0,\dots,N} E(n, 60000, t_k).$$
(3.10)

An index of gain deflection associated with changing the initial load from $q_0^1 \in Q_0$ up to $q_0^2 \in Q_0$ is defined as follows

$$I(n, q_0^1, q_0^2) = E_T(n, q_0^2)/E_T(n, q_0^1).$$
(3.11)

Observe that indicator (3.11) is nothing but an index of elasticity of the threshold norm of the initial load from q_0^1 to $[q_0^2$ [13].

We apply formula (3.11) to the given volumes of the initial load from $q_0^1 \in Q_0$ to $q_0^2 \in Q_0$ (those two arguments are omitted in further notation):

$$I(n) = E_T(n, 60000)/E_T(n, 500).$$
(3.12)

Further analysis of the transition into chaos is carried out graphically (see Figs. 3.1 and 3.2) using indicators (3.8) and (3.11).

3.3. Computational experiment

In order to detect a chaotic regime, formulas (3.9) and (3.10) are applied. If the elasticity of deflection monotonically changes with an increasing number of partitions, then a chaotic regime should not appear. However, the latter conclusion requires additional investigations, since the applied method depends on the initial data. In fact, it supplements the classical method of analysis described in Section 3.2. If the elasticity of deflection has a stepwise shape, then the presence of a chaotic process is doubtful.

The Fig. 3.1 shows pattern of changes in elasticity versus n. The left column refers to the data, whereas the right column presents the graphical representation in the case of regular (a) and chaotic (b) dynamics. Both regression lines were obtained using the least squares method.

The elasticity indices shown in Tables 4 and 5 are computed using the following algorithm. **Step 1.** We take initial parameters. We fixed here $\omega_p = 5$ (in what follows in Figs. 3.2 and 3.3 the computations are demonstrated also for $\omega_p = 2.5$). **Step 2.** We fix the initial load (here $q_0 = 500$ and $q_0 = 60000$). **Step 3.** We construct the mesh, where $n + 1$ denotes the number of nodes (see Section 2.1). In the experiment $n = 60, 80, 84, 88, 90, 94, 98, 100, 120$. **Step 4.** For each t deflection w

(a)

n	$E_T(n,500)$
60	0.0000135
80	0.0000645
84	0.0000728
88	0.0000750
90	0.0000771
94	0.0000804
98	0.0000789
100	0.0000768
120	0.0000714

(b)

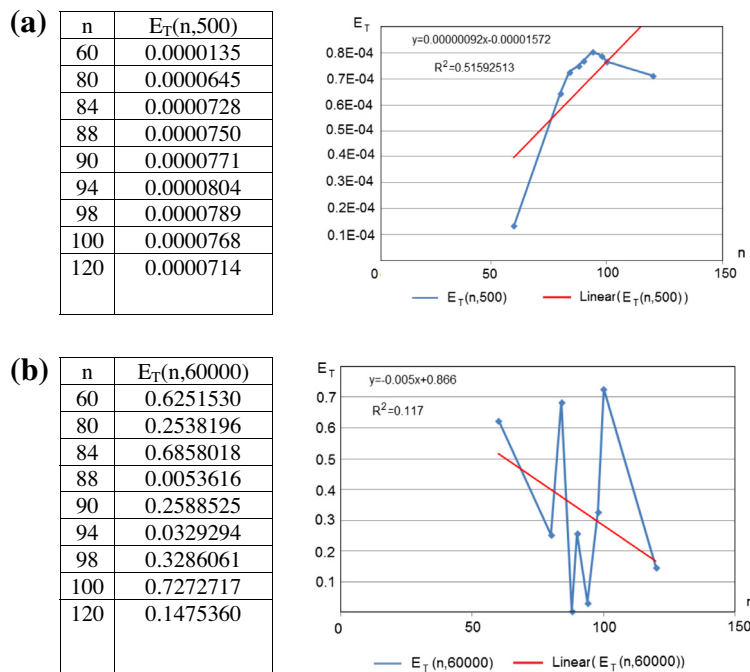| n	$E_T(n,60000)$
60	0.6251530
80	0.2538196
84	0.6858018
88	0.0053616
90	0.2588525
94	0.0329294
98	0.3286061
100	0.7272717
120	0.1475360

Fig. 3.1. The elasticity E_T harmonic (a) and chaotic (b), including data (left column) and graphical representation (right column).
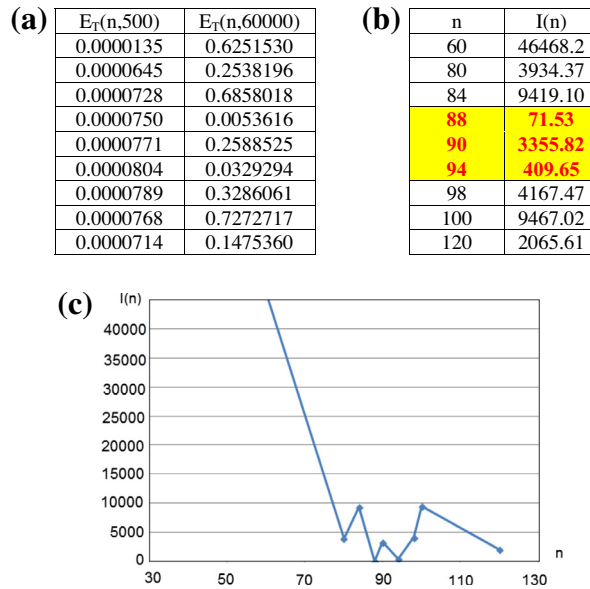
(a)

$E_T(n,500)$	$E_T(n,60000)$
0.0000135	0.6251530
0.0000645	0.2538196
0.0000728	0.6858018
0.0000750	0.0053616
0.0000771	0.2588525
0.0000804	0.0329294
0.0000789	0.3286061
0.0000768	0.7272717
0.0000714	0.1475360

(b)

n	I(n)
60	46468.2
80	3934.37
84	9419.10
88	**71.53**
90	**3355.82**
94	**409.65**
98	4167.47
100	9467.02
120	2065.61

(c)

Fig. 3.2. Critical zone estimation via E_T (a), $I(n)$ (b, c) $n \in [88 : 94]$.

(a)

$E_T(n,500)$	$E_T(n,60000)$
0.0000677	0.0000000
0.0000671	0.2188168
0.0000701	0.5000161
0.0000720	1.8169283
0.0000728	0.0057437
0.0000740	0.5186395
0.0000748	0.0369340
0.0000752	2.0703852
0.0000729	0.0053920

(b)

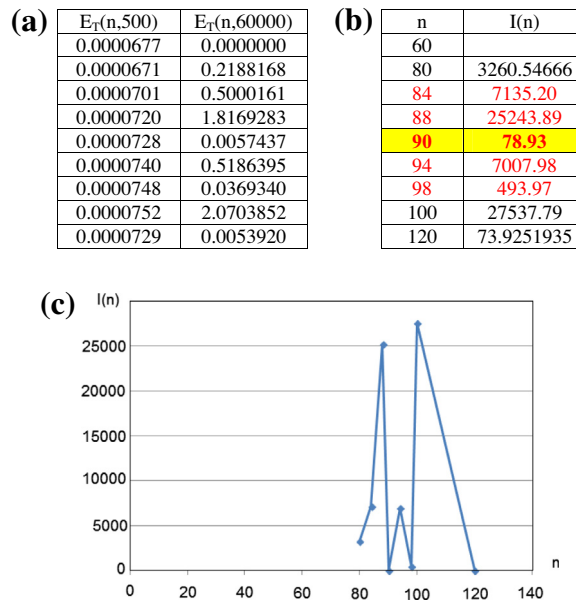| n	I(n)
60	
80	3260.54666
84	7135.20
88	25243.89
90	**78.93**
94	7007.98
98	493.97
100	27537.79
120	73.9251935

(c)

Fig. 3.3. Critical zone estimation via E_T (a), $I(n)$ (b, c) $n \in [84 : 98]$.

is fixed. A simple computation of load q for each t and for the earlier defined fixed parameters is carried out using the formula $q = q_0 \sin(\omega_p t)$. As a result, all data required by formulas (3.9) and (3.10) are obtained. The assumed values of t are denoted as $t_0, t_1, \ldots, t_N$. The observation time instant is ordered in the following way: $T = \{t_0 < t_1 < \cdots < t_N\}$. **Step 5.** Basic indies are estimated by data (3.3) and (3.5), and their moduli (3.4) and (3.6) are taken. **Step 6.** We use formula (3.7), i.e. we get

$$E(n, 500, t_k) = \frac{w(n, 500, t_k)/w(n, 500, t_0) - 1}{q(n, 500, t_k)/q(n, 500, t_0) - 1},$$

$$E(n, 60000, t_k) = \frac{w(n, 60000, t_k)/w(n, 60000, t_0) - 1}{q(n, 60000, t_k)/q(n, 60000, t_0) - 1}.$$

Step 7. In order to find the elasticity indices we apply formulas (3.9) and (3.10). The earlier described algorithm steps are shown in Fig. 3.1 for different n.

Typically, the increase of n reduces differences between the deflection index at high and low load values.

If this trend begins to change dramatically, the process migrates to the area of noise, and the choropleth map (Tables 1–3) cannot give a correct picture of the fluctuations.

Step 8. Index I is computed using formula (3.12). The interval of n which includes one or more consecutive jumps of index (3.12) would be referred to as the critical area (see Fig. 3.2) and is marked by yellow color.

Below, the so far described algorithm is applied to a second beam vibration regime (for $\omega_p = 2.5$). The elasticity indicator E_T and index gain deflection $I(n)$ (Fig. 3.3) show that for $n = 60$ the dependence of the load deflection is much less than 5% (0.05) and harmonic vibrations take place for $q_0 = 500$ and for $q_0 = 60000$.

4. Concluding remarks

First of all it should be mentioned that in the case of many coupled non-linear oscillators (the number of second order non-linear ODEs is 60, 80, 100 or 120) it is rather equally difficult to find any of the mentioned attractors, i.e. either regular (periodic and quasi-periodic) or chaotic ones. This observation regarding structural members (beams, plates and shells) can be found in references [6,22,23], where the so called charts of vibration types have been reported. In those charts the zones of existence of regular, chaotic and bifurcation dynamics on the chosen planes of parameters are comparable with respect to their areas/magnitudes. Furthermore, the same observation holds even for a triple pendulum (see [11]). In the latter case we have an experimental rig and again the strongly nonlinear mechanical system exhibits rich non-linear dynamical phenomena. In other words, in the latter case it is rather difficult to find regular attractors since chaotic dynamics is dominating.

We have proposed a system of indexing procedure based on a formal computation and collection of the elasticity indicator (usually applied in the mathematical economy) in order to determine the parameters of transition of the flexible curved beams into a chaotic vibrational regime. The proposed new approach allows us to avoid the disadvantages of the classical methods, i.e.:

(i) complexity of the analyzed attractor is reduced essentially owing to the introduction of numerical indexing parameters (here $I(n)$ and $E_T(n, q_o)$);
(ii) dynamics of the deflection intensity indicator E_p does not depend essentially on the number of partition n;
(iii) there is no need of earlier identification of the vibrational regime.

Furthermore, the so far obtained results are promising and can also be applied directly to quantify various real physical processes through the efficient saving of the computational time required for the analysis of different regimes of attractors while solving numerically ordinary differential equations.

Acknowledgement

References

[1] Jacobs G, Šlaus I. Indicators of economics progress: the power of measurement and human welfare. CADMUS J 2010;1(1):53–113.
[2] Drożdż S, Grümmer F, Ruf F, Speth J. Towards identifying the world stock market cross-correlations: DAX versus Dow Jones. Physica A 2001;294(1):226–34.
[3] Bastos JA, Caiado J. Recurrence quantification analysis of global stock markets. Physica A 2011;390(7):1315.
[4] Bevilacqua F, Van Zon A. Random walks and non-linear paths in macroeconomic time series: some evidence and implications. In: Foster J, Hölzl W, editors. Applied evolutionary economics and complex systems. Cheltenham, Northampton: Edward Elgar Publishing; 2004. p. 36–77.
[5] Awrejcewicz J, Krysko VA, Krysko AV. Thermo-dynamics of plates and shells. Berlin: Springer-Verlag; 2007.
[6] Awrejcewicz J, Krysko VA. Chaos in structural mechanics. Berlin: Springer-Verlag; 2008.
[7] Kyrtsou C, Vorlow C. Modelling non-linear comovements between time series. J Macroecon 2009;31:200–11.
[8] Faggini M. Chaos detection in economic time series: metric versus topological tools. Adv Manage Appl Econ 2013;3(6):27–52.
[9] Nigmatullin RR, Machado JT, Menezes R. Self-similarity principle: the reduced description of randomness. Cent Eur J Phys 2013;11(6):724–39.
[10] Nigmatullin RR, Khamzin AA, Machado JT. Detection of quasi-periodic processes in complex systems: how do we quantitatively describe their properties? Phys Scr 2014;89(1):015201.
[11] Nigmatullin RR, Osokin SI, Awrejcewicz J, Kudra G. Application of the generalized Prony spectrum for extraction of information hidden in chaotic trajectories of triple pendulum. Central Eur J Phys 2014:1–21.
[12] Leonov GA. Strange attractors and classical stability theory. St. Petersburg: St. Petersburg University Press; 2008.
[13] Pindyck RS, Rubinfeld DL. Microeconomics. New York: Prentice-Hall; 2001.
[14] Verian KhR. Microeconomics today. Moscow: Mir; 1997.
[15] Vygodchikova IYu. On the method of approximation of the economic data using the Chebyshev's problem and its generalization. Izviestiya of Saratov National University. Series of Economics Control Law 2012;12(1):77–80. in Russian.
[16] Abrams DM, Strogatz SH. Chimera states in a ring of nonlocally coupled oscillators. Int J Bifurcation Chaos 2006;16:21–37.
[17] Omel'chenko OE, Maistrenko YL, Tass PA. Chimera states: the natural link between coherence and incoherence. Phys Rev Lett 2008;100:044105.
[18] Kuramoto Y, Battogtokh D. Coexistence of coherence and incoherence in nonlocally coupled phase oscillators. Nonlinear Phenom Complex Syst 2002;5:380–5.
[19] Shima S, Kuramoto Y. Rotating spiral waves with phase-randomized core in nonlocally coupled oscillators. Phys Rev E 2004;69(3):036213.
[20] Ko TW, Ermentrout GB. Partially locked states in coupled oscillators due to inhomogeneous coupling. Phys Rev E 2008;78(1):016203.

[21] Laing CR. Chimera states in heterogeneous networks. Chaos 2009;19:013113.
[22] Krysko AV, Awrejcewicz J, Kutepov IE, Zagniboroda NA, Dobriyan V, Krysko VA. Chaotic dynamics of flexible Euler–Bernoulli beams. Chaos 2014;34(4):043130.
[23] Krysko AV, Awrejcewicz J, Saltykova OA, Zhigalov MV, Krysko VA. Investigations of chaotic dynamics of multi-layer beams using rotational inertial effects. Commun Nonlinear Sci Numer Simul 2014;19(8):2568–89.